

Linear Chains of Styrene and Methyl-Styrene Molecules and their Heterojunctions on Silicon: Theory and Experiment

George Kirczenow

Department of Physics, Simon Fraser University, Burnaby, British Columbia, Canada V5A 1S6

Paul G. Piva and Robert A. Wolkow

National Institute for Nanotechnology, National Research Council of Canada,

Edmonton, Alberta T6G 2V4, Canada, and Department of Physics,

University of Alberta, Edmonton, Alberta T6G 2J1, Canada

(Dated: March 23, 2022)

We report on the synthesis, STM imaging and theoretical studies of the structure, electronic structure and transport properties of linear chains of styrene and methyl-styrene molecules and their heterojunctions on hydrogen-terminated dimerized silicon (001) surfaces. The theory presented here accounts for the essential features of the experimental STM data including the nature of the corrugation observed along the molecular chains and the pronounced changes in the contrast between the styrene and methyl-styrene parts of the molecular chains that are observed as the applied bias is varied. The observed evolution with applied bias of the STM profiles near the ends of the molecular chains is also explained. Calculations are also presented of electron transport along styrene linear chains adsorbed on the silicon surface at energies in the vicinity of the molecular HOMO and LUMO levels. For short styrene chains this lateral transport is found to be due primarily to direct electron transmission from molecule to molecule rather than through the silicon substrate, especially in the molecular LUMO band. Differences between the calculated position-dependences of the STM current around a junction of styrene and methyl-styrene molecular chains under positive and negative tip bias are related to the nature of lateral electron transmission along the molecular chains and to the formation in the LUMO band of an electronic state localized around the heterojunction.

PACS numbers: 85.65.+h, 81.07.Pr, 73.63.-b, 73.22.-f

I. INTRODUCTION

During the last few years there has been growing interest in molecular electronics, stimulated largely by the experimental realization of molecular wires,^{1,2,3} systems in which a single organic molecule or a few molecules carry an electric current between a pair of metal contacts. In some cases such systems exhibit switching behavior and/or negative differential resistance,^{4,5,6} phenomena that may be exploited in future molecular electronic devices. Hybrid molecular/semiconductor nano-electronic devices are another intriguing possibility and fundamental research that may ultimately lead to their creation is also being pursued at the present time.^{7,8,9,10,11,12,13,14} Recently, techniques have been developed that make it possible to grow an oriented linear chain of styrene molecules on a hydrogen-terminated silicon substrate beginning at a predefined point on the substrate.^{8,12} The electronic structure and STM images of these homomolecular chains of styrene have also been modelled theoretically.^{9,10} However, no studies (experimental or theoretical) of chains of styrene molecules with chemical substituents attached have been reported to date. In the work reported in the present article we extend the experiments and theory to a related system, a *heteromolecular* chain of molecules on a silicon substrate where the chemical identity of the molecular species changes abruptly across a heterojunction from styrene to methyl-styrene. As the chemical composition across the molecular chain

varies solely by the presence (or absence) of a substituent (in this case a methyl group) on the aromatic ring, the π - π^* stacking that is an essential prerequisite for wire-like conduction along the chain remains undisrupted.

Some intriguing questions regarding the self-assembled lines of molecules on silicon are: To what extent do the molecules that form the line communicate with each other electronically? Is electrical conduction along the line possible, and if so is such conduction dominated by transport through the molecules themselves or through the silicon substrate? Calculations of lateral transport along the molecular chain can in principle answer these questions. However, to date such calculations have not been reported for molecular chains on silicon, although molecular band formation in the styrene chains due to orbital overlap between molecules has been studied,^{9,10} as has conduction through stacks of aromatic biphenyldithiol molecules not attached to a substrate.¹⁵ The role of molecule-molecule interactions in vertical conduction through molecules between metal contacts has also been investigated theoretically.^{16,17,18,19,20}

To date it has not been feasible experimentally to connect a pair of probes to the two ends of a chain of molecules on silicon so as to measure the lateral transport directly: STM studies of the molecular chains measure vertical transport between the silicon substrate and a single metal tip via the adsorbed molecules.^{8,12} However, vertical transport measurements may yield indirect experimental information relevant to lateral transport, particularly if the molecular chain is inhomoge-

neous. A heterojunction between chains of similar but distinct molecules such as styrene and methyl-styrene on silicon or the end of a line of molecules may be a suitable inhomogeneity for such studies, but theoretical modeling of such systems is clearly needed in order to extract meaningful information of this kind from experimental data.

A realistic model is presented here of the structure, electronic structure and electronic transport in chains of styrene and methyl-styrene molecules on hydrogen-terminated dimerized silicon (001) surfaces. The model accounts for the main properties of heterojunctions of styrene and methyl-styrene molecular chains on silicon that have been observed in our STM experiments, as well as the experimentally observed phenomena associated with the ends of the molecular lines. The first calculations are presented of lateral transport through short styrene chains adsorbed on the silicon surface. It is found that lateral electron transport along an 8-molecule styrene chain at energies corresponding to the molecular HOMO and LUMO bands is primarily due to direct electron transmission from molecule to molecule rather than transmission via the silicon substrate. This dominance of molecule-to-molecule transmission over transmission through the substrate is stronger for the LUMO band than the HOMO band. This difference is related to pronounced differences between the calculated position-dependences of the STM (vertical transport) current around the junction of styrene and methyl-styrene molecular chains under positive and negative tip bias.

This article is organized as follows: In Section II we present experimental results detailing the growth and STM imaging characteristics of heteromolecular chains of styrene and methyl-styrene on silicon. In Sections III and IV we describe our modeling of the structure and electronic structure of the molecular chains. The approach used in our transport calculations is summarized in Section V. Our theoretical results for vertical transport in the STM geometry in the vicinity of a heterojunction of molecular lines are presented and compared with experiment in Section VI. Our theoretical results regarding lateral transport along the molecular chains and how this may influence STM images are presented in Section VII. Our experimental and theoretical findings regarding the structure and STM images of the ends of the molecular chains are discussed in Section VIII. Finally, our conclusions are summarized in Section IX.

II. EXPERIMENT

The experiments were performed on a hydrogen terminated Si(100)-2×1 surface. Samples were cleaved from an arsenic-doped (0.005 Ω·cm) Si (100) oriented wafer, mounted in molybdenum sample holders, and load-locked into an ultrahigh vacuum (UHV) chamber (background system pressure < 1×10⁻¹⁰ Torr). Samples were degassed for 8 hours at 700°C. Removal of the surface oxide,

and sublimation/replanarisation of the surface layers was achieved by repeated thermal cycling to 1250°C. Sample temperatures were monitored using a calibrated infrared pyrometer. During the annealing procedure, sample heating was discontinued if at any point the monitored system pressure exceeded 4×10⁻¹⁰ Torr. This sample preparation method produces 100 oriented silicon surfaces with well ordered silicon terraces (2×1 surface reconstruction), and a surface defect concentration below 5%.

The vacuum preparation chamber was then filled with hydrogen gas (1×10⁻⁶ Torr), and a hot tungsten filament (T ~ 1600°C) situated 10 cm from the sample was used to provide a flux of reactive atomic hydrogen to the surface. The sample was heated to 330°C and exposed to the atomic hydrogen flux for 13 minutes. These conditions allowed the formation of a quasi-saturated monolayer of silicon monohydride with a 2×1 surface reconstruction.²¹

One-dimensional molecular organic heterowires were grown along dimer rows of the as-prepared H:Si (100) surfaces using a vacuum phase reaction studied earlier by Lopinski and co-workers.⁸ In the case of the styrene reaction with the H:Si surface, the double carbon bond in the vinyl group at the base of styrene molecule reacts with a surface silicon radical (corresponding to a hydrogen vacancy on the H:Si surface) to produce a silicon-carbon bond and a carbon radical (centred on the carbon atom bound to the aromatic ring). The carbon centred radical then abstracts a hydrogen atom from an adjacent dimer on the same row (and from the same side of the dimer - never from the other (diagonal) atom), producing a newly reactive site. Successive reactions lead to the well ordered linear structures reported in Ref. 8. Several substituted styrene compounds have been studied in our group and have demonstrated this self-directed line growth mechanism on H:silicon.²² Here two such compounds are used, styrene and 4-methyl-styrene, to fabricate one-dimensional organic heterowires.

On the H:Si(100) surface, residual silicon radicals typically exist at the level of a few percent and are used in this work as initiation sites for the self-directed growth of 4-methyl-styrene/styrene heterowires. The molecular heterowires were fabricated by sequentially introducing 4-methyl-styrene and styrene into the STM chamber through a variable leak valve. Dissolved atmospheric gases in the styrene and 4-methyl-styrene were expelled from the liquid phase samples by repeated freeze-pump-thaw cycles. Prior to dosing, the STM tip was retracted ~ 1 micrometer from the H:silicon surface. During dosing, the flow of vapour phase reactant was adjusted to bring the chamber pressure to ~ 4×10⁻⁷ Torr, and held for several tens of seconds (integrated doses given below). After dosing (valve shut), the chamber pressure returned below 1×10⁻¹⁰ Torr.

Images of the H:Si(100) surfaces were collected in UHV at room temperature using an Omicron STM1. Electrochemically etched tungsten tips were cleaned in-situ by electron beam bombardment and field emission prior to

STM imaging. Constant current topographic STM images were acquired using a constant tunnel current of 60 pA. Quoted dimensions along the lateral and vertical directions have been scaled to agree with known values for the silicon dimer spacing, and silicon terrace height, respectively. 4-methyl-styrene/styrene heterostructures were grown on several H-silicon surfaces, and studied with different STM tips.

Figs. 1 and 2 show the growth and bias-dependent filled-state imaging of a methyl-styrene/styrene heterostructure. Fig.1(a), acquired using a sample voltage (V_s) of -3.0 V, shows the formation of the first line segment following a 8 Langmuir dose of methyl-styrene (1 Langmuir = 10^{-6} Torr-seconds). Approximately 8 molecules of methyl-styrene have reacted at the indicated location. The bright feature at the end of the line segment (indicated by the white arrow) corresponds to the terminal silicon radical (i.e. a bare silicon atom which has transferred its hydrogen atom to the adjacent methyl-styrene molecule). Its presence indicates that the reaction between the methyl-styrene and the silicon surface at this particular site has not reached saturation.

Fig.1(b) shows the same region of the crystal following a 78 Langmuir exposure of styrene. Starting at the silicon radical in (a), approximately 8 molecules of styrene have subsequently reacted to form a methyl-styrene/styrene heterostructure. The location of the heterointerface is indicated by the white wedge. The silicon radical present in (a) is absent from the end of the styrene line segment in panel (b), and in panels (c) and (d) acquired at lower magnitude bias. This suggests that linegrowth has terminated at an unresolved surface defect (such as a dihydride site), or has been capped by a H-atom deposited by the STM tip.²³

Panels (b) - (d) show the topographic envelope of the heterostructure at varying sample bias. At $V_s = -3.0$ V [panel (b)], the constant current contours follow a relatively smooth envelope modulated by the physical height of the methyl-styrene and styrene line segments above the H:silicon surface. At this value of the bias the aromatic π states in the styrene and methyl-styrene lie above the tip Fermi-level. The tunnel current therefore results from electrons which tunnel from underlying occupied states within both the silicon and surface bound molecules into empty states within the STM tip. The extent to which molecular orbital states emptied by tunneling are replenished directly by underlying silicon states (i.e. vertical transport across molecules) or indirectly by nearest neighbour molecules (reflecting a degree of lateral transport across the molecular chain) is considered in the following theory sections.

In panel (c) [$V_s = -2.4$ V], the aromatic π states move below the tip Fermi-level, and the imaging current is supplied by silicon states which tunnel across the surface bound molecules. In this regime, the methyl-styrene and styrene image with similar height. Also, molecular scale corrugation appears within the topographic envelope. In panel (d) [$V_s = -1.8$ V], the molecular corrugation shows

different contrast between the methyl-styrene and styrene line segments.

To better resolve differences in the imaging characteristics between both segments, 0.2 nm wide topographic cross-sections were extracted along two parallel axes within the heterostructure envelope. Images were registered using a least squares fitting algorithm to allow extraction of cross-sections from nominally identical locations between images acquired at different bias.

Cross-sections taken along the direction of the blue arrow (Fig.1 panel (d) inset) appear in panel (a) of Fig.2 and are centred above the chemical attachment points between the heterostructure and the underlying dimer row. Cross-sections taken along the direction of the red arrow, appear in panel (b) of Fig.2, and are centred to the right of the trench separating the underlying dimer rows. Cross-sectional data extracted from images (not shown) acquired at sample voltages of -2.0 V, -2.2 V, -2.6 V, and -2.8 V have been added to the data presented in Fig.2.

In panels (a) and (b) of Fig.2, the height envelope corresponding to the methyl-styrene line segment is situated between 2.5 nm and 6.0 nm along the distance axis. The styrene line segment is situated between 6.0 nm and 9.8 nm. The peaks centred at 1.5 nm (in both panels) and at 10.3 nm (in panel (a) only) correspond to the isolated (and unidentified) structures present in the upper and lower left hand corners of the images in Fig.1.

In each panel the position of the corrugation maximum associated with the interfacial methyl-styrene molecule is indicated by a black arrow. The position of the chemical interface in the heterowire is made evident by the differential height contrast observed between the two line segments at high and low bias. Superposition of the heterowire envelope with registered cross-sections extracted from Fig.1 (a) (not shown) agree with this determination. In this case, the topographic maximum (i.e. the silicon radical) at the end of the methyl-styrene segment in Fig.1 (a) lies between the as-identified interfacial methyl-styrene and styrene corrugation maxima in the completely grown heterowire. Other methyl-styrene/styrene heterowires studied displayed similar agreement between the apparent and expected locations of the heterojunction.

The main features displayed in Fig.1 are visible in the cross-sectional data presented in panels (a) and (b) of Fig.2. As the magnitude of the imaging bias is increased, the apparent height of the methyl-styrene and styrene line segments increases and begins to saturate (with methyl-styrene imaging above styrene). At low magnitude bias (where the contribution of molecular π states to the tunnel current is suppressed), the molecular corrugation is more apparent.

While in panel (b) the height of the methyl-styrene line segment is comparable to (at low magnitude bias) or greater than (at high bias) that of styrene, a different behaviour is observed along the chemical attachment points in (a). At low magnitude bias, $|V| < 2.6$

V, the methyl-styrene molecules image lower than the styrene molecules. Given that methyl-styrene extends farther beyond the H:silicon surface than styrene, and the similarity in molecular conformation anticipated for the molecules in each segment, this observation seems unexpected.

At the heterojunction, the imaging contrast between the interfacial molecules (styrene and methyl-styrene) appears to a first approximation comparable to the contrast resolved for these same molecules within their respective line segments. A significant departure from this behaviour is observed at elevated magnitude bias ($|V| \gtrsim 2.6$ V), where the interfacial methyl-styrene appears lower than the molecules located within the line segment. The molecules at either end of heterowire also image with decreased height. Finally, a slight upward bowing (roughly centred at the heterointerface) appears superimposed on the bulk of the cross-sectional curves.

In the absence of electronic interaction between molecules and geometrical differences between them, every molecule along a homomolecular wire (or a homomolecular line segment in the case of a heterowire) would image with identical properties. This is not observed. The implication is that the observed height profiles along the heterowire reflect some combination of: i) conformational changes in the molecules along the chain due to intermolecular forces, ii) dispersion interactions leading to differential broadening and shifting of molecular electronic levels along the chain, and/or iii) tunneling current collected by the STM tip above a given molecule receiving contributions from neighbouring molecules along the chain reflecting some degree of lateral current transport across the stacked aromatic rings.

To determine the origin of the observed contrast in molecular corrugation, and the topographic height variations resolved along the heterowire structure, a theoretical model for the heterowire is developed and its current transport properties are considered in sections IV to VIII.

III. MODELING THE STRUCTURE

The spacing between the tops of the molecules seen in our experimental STM images of styrene/methyl-styrene chains on the (001) silicon surface varies along the length of the chain and is larger near the ends of the chain than near its center. Because of the variable mismatch between the molecular spacing and the underlying silicon lattice, it is not appropriate to model these molecular chains theoretically as structures periodic along the length of the chain with a small unit cell. They are therefore modelled here as finite clusters such as that depicted in Fig.3 which shows a molecular chain with a heterojunction, consisting of four styrene and four methyl-styrene molecules. The molecules bond to a dimerized Si (001) surface that is represented by two rows each of 10 silicon dimers together with four underlying atomic layers of silicon atoms. All of the dangling bonds are passivated

with hydrogen. The lowest carbon atom of each molecule bonds to a surface Si atom and the molecules lean over the “trench” between the two rows of silicon dimers.²⁵

A complete *ab initio* relaxation of this cluster using Kohn-Sham density functional theory would be impractical, so the following hybrid approach was adopted to calculate its approximate structure: An *ab initio* density functional relaxation was carried out²⁷ of a smaller cluster consisting of one styrene and one methyl-styrene molecule over two rows each of two silicon dimers, with two additional underlying layers of silicon, all of the dangling bonds passivated with hydrogen. This small cluster shown in Fig.4 is similar to the immediate vicinity of the junction between styrene and methyl-styrene chains in Fig.3. The relaxation of this small cluster was carried out keeping the atoms of the two lower silicon layers fixed at positions corresponding to a bulk silicon crystal lattice but allowing the positions of all of the atoms of the molecules, the silicon dimer atoms and all of the hydrogen atoms to relax freely. The main difference between the relaxed geometries of the two molecules in Fig.4 and that of an *isolated* molecule bound to the same silicon site is that the two molecules tilt somewhat away from each other. This tilt occurs mainly through changes in the sequence of dihedral angles defined (in the Z-matrix description of the system) by the orientations of the bonds connecting Si atom 1 to C atom 2, C atom 2 to C atom 3, and so on along the carbon atom chain through C atom 6 of the styrene molecule (see Fig.4), and of the corresponding bonds of the methyl-styrene molecule. Thus the relaxed geometry of the cluster in Fig.3 was generated by assigning initially to all of the atoms of the molecules positions derived from the relaxed geometries of the respective atoms of the smaller cluster in Fig.4. Then this initial structure was relaxed so as to minimize the energy of the cluster using the AM1 empirical model,²⁸ but allowing *only* the above dihedral angles, the dihedral angles defining the orientations of the C-H bonds involving carbon atoms 2 and 3 and corresponding C-H bonds on other molecules, and the dihedral angles defining the orientation of the triplets of H atoms belonging to the methyl groups to vary. During the AM1 relaxation a further constraint was also imposed, namely, that the tilts of the styrene and methyl-styrene molecules at the ends of the 8 molecule chain be such that the average lateral spacing between the top carbon atoms of the molecules approximate the experimentally observed average spacing of the molecules near the junction of the styrene and methyl-styrene chains.²⁹ The final model geometry of the 8 molecule chain is thus representative of the region of a much longer molecular chain around the heterojunction. A similar procedure was used to obtain the relaxed geometry of the chain of 8 styrene molecules used in the theoretical studies of lateral electron transport along the molecular chain that are discussed in Section VII. However, the structures used in our theoretical studies of the ends of the molecular chains were obtained somewhat differently as is described in Section VIII. Finally, it

was found that the energy of the structure with methylstyrene molecules varies by much less than kT (where T = room temperature) when the methyl groups are rotated about the bonds connecting them to the benzene rings of the molecules. Since the experiments on these systems were carried out at room temperature, the calculated STM tip currents presented below are averages over orientations of the methyl groups.

The atomic structure of the tungsten STM tip in our experiments is unknown and the tip was modelled arbitrarily as a (001)-oriented (relative to the (001) Si surface) clean bcc tungsten tip terminating in a single tungsten atom. A total of 15 tungsten atoms arranged in layers of 1,4,5,4 and 1 atoms along the (001) direction were included in the model of the tip. These atoms were placed at their nominal positions in a bulk bcc tungsten lattice except for the terminal atom whose position was relaxed along the (001) direction (towards the center of the tungsten cluster) so as to minimize the Kohn-Sham energy of the 15 atom tungsten cluster.³⁰ The effect of an alternate tip on the calculated STM currents, obtained by replacing the apex atom with a single silicon atom whose position was relaxed appropriately, was also investigated.

IV. MODELING THE ELECTRONIC STRUCTURE

Most theoretical work on electronic transport in molecular wires with metal contacts has been based on semi-empirical tight-binding models or *ab initio* Kohn-Sham density functional calculations of the electronic structure.^{3,31,32,33,34,35,36} However, the atomic structures of the molecule-metal junctions are not known. Thus, with a few exceptions,^{36,37} comparison of theoretical predictions with experiments on metal/molecule/metal wires is subject to large uncertainties. By contrast, the bonding geometries of many small organic molecules to silicon substrates are known,⁷ as are the specific atomic silicon sites involved in the carbon-silicon bonds anchoring styrene and methylstyrene molecular chains to the silicon.^{8,9,10,14} Thus comparison between theory and experiment is subject to much less uncertainty for these molecules on silicon than for metal/molecule/metal wires. This allows us to assess the validity of different models of the electronic structure of the molecular chains on silicon by comparison with experimental data.

Previous theoretical work modeling the current-voltage characteristics of single styrene molecules on silicon found *ab initio* Kohn-Sham density functional calculations unsuitable for treating the electronic structure of the silicon substrate.¹³ The present work on styrene and methylstyrene chains on silicon reached a similar conclusion: Our density functional calculations that employed localized orbital bases appropriate for quantum chemistry²⁷, in common with previous density functional calculations for styrene chains on silicon that employed plane wave

bases,¹⁰ yielded molecular HOMO levels aligned with the highest occupied silicon valence states. This level alignment is unrealistic; experimentally the molecular HOMO energy is considerably lower. Furthermore, if it were correct then STM images of the styrene molecules probing occupied states at low bias would show a current node at the center of each molecule since the molecular HOMO is a π -like orbital on the benzene ring. However, this is not seen experimentally. Finally, density functional calculations in the local density approximation seriously underestimate the band gap of *bulk* silicon. For these reasons³⁸ a different approach based on extended Hückel theory will be adopted here in modeling the electronic structure of the molecules, the silicon substrate and the tungsten STM tip. Our model corrects the above deficiencies of density functional theory and yields current *maxima* over the centers of the molecules for low negative applied substrate bias, consistent with the nature of the corrugation along the molecular chain that is observed experimentally.

Extended Hückel theory is a semi-empirical tight binding scheme from quantum chemistry that provides an approximate description of the electronic structure of many molecules. It describes molecular systems in terms of a small set of Slater-type atomic orbitals $\{|\phi_i\rangle\}$, their overlaps $S_{ij} = \langle\phi_i|\phi_j\rangle$ and a Hamiltonian matrix $H_{ij} = \langle\phi_i|H|\phi_j\rangle$. The diagonal Hamiltonian elements $H_{ii} = \epsilon_i$ are chosen to be the atomic orbital ionization energies. In the Wolfsberg-Helmholz form of the model, the non-diagonal elements are approximated by

$$H_{ij} = KS_{ij}(\epsilon_i + \epsilon_j)/2 \quad (1)$$

where K is a phenomenological parameter usually chosen to be 1.75 for consistency with experimental molecular electronic structure data. The extended Hückel model has been used successfully to explain the experimental current-voltage characteristics of a variety of molecular wires connecting metal electrodes.^{3,32,34} However, without modification it is unsatisfactory for crystalline silicon as it predicts a band gap that is direct and roughly three times larger than that found experimentally for this material. In the present work these deficiencies of the extended Hückel model have been corrected by replacing equation (1) for the Hamiltonian matrix elements between the atomic orbitals of silicon by

$$H_{ij} = K_{ij}S_{ij}(\epsilon_i + \epsilon_j)/2 \quad (2)$$

where the K_{ij} are fitting parameters⁴⁰ chosen so that the modified extended Hückel model obtained in this way yields the correct silicon band structure. The extended Hückel Hamiltonian matrix elements for tungsten were adjusted similarly so as to match the band structure of bcc tungsten,⁴¹ however in the case of tungsten some modification of the extended Hückel model's orbital energies ϵ_i was also found to be necessary to achieve a good fit. Finally a realistic alignment between the molecular HOMO level and the Fermi levels of the silicon and

tungsten clusters was achieved by shifting the silicon and tungsten orbital energies ϵ_i by appropriate amounts E_{Si} and E_W respectively.⁴¹ Because of the non-orthogonality of the extended Hückel basis states, such shifts of the diagonal matrix elements of the Hamiltonian also require⁴² corresponding shifts ΔH_{ij} of the non-diagonal elements H_{ij} , which were taken to be

$$\Delta H_{ij} = S_{ij}(E_i + E_j)/2 \quad (3)$$

where $E_k = E_{Si}$ or E_W if $\{|\phi_k\rangle\}$ is a silicon or tungsten orbital, respectively.

Fig.5 shows the key features of the electronic structure of the eight-molecule styrene/methyl-styrene heterojunction on the hydrogen passivated silicon cluster whose geometry is depicted in Fig.3, as described by the above electronic structure model: The energy eigenvalues and eigenstates of the model Hamiltonian were calculated and a Mulliken analysis was carried out to determine the silicon, carbon and hydrogen content of each eigenstate. The carbon content was further resolved according to whether the carbon atom belongs to a styrene or methyl-styrene molecule. The results are shown as histograms in Fig.5 a (Si), b (C/styrene), c (C/methyl-styrene) and d (H), summed for the sake of clarity over the eigenstates in bins of energy of width 0.1 eV. The vertical line labelled “Si HOMO” marks the energy of the highest occupied state of the cluster which has mainly silicon content. The carbon band below about -12.3 eV corresponds to molecular HOMO orbitals while the carbon band around -8.2 eV corresponds to the molecular LUMO. Because the HOMO (LUMO) of ethylbenzene is close in energy and generally similar to the HOMO (LUMO) of methylethylbenzene, the molecular HOMO (LUMO) bands due to the styrene and methyl-styrene on silicon (Fig.5b and c) are similar to each other although the styrene band edges are slightly lower (by ~ 0.1 -0.2 eV) in energy than those for methyl-styrene.

Note also the weak carbon features between the molecular HOMO band edge at -12.3 eV and the (mainly silicon) cluster HOMO at -11.3 eV. These are almost identical for the styrene and methyl-styrene molecules and are due to electron tunneling through the molecules from occupied states of the silicon substrate that lie above the molecular HOMO band. This tunneling is responsible for the STM current for low negative sample bias at which the experimentally observed STM images of the molecules are similar to those calculated using the present model (Fig.6 plot L in Section VI) but differ markedly from the those predicted by density functional calculations as was discussed above.

Since the styrene and methyl-styrene molecules are coupled more strongly to the silicon substrate than to the STM tip, it is assumed for simplicity in the present work that when a bias voltage V is applied between the STM tip and sample, the entire voltage drop occurs between the molecules and the STM tip.⁴³ The corresponding shift eV of the energy levels of the tip relative to the sample is then included in E_W , and thus also contributes

to the off-diagonal matrix elements of the Hamiltonian through equation (3).

Finally, it should be emphasized that because the present model includes only a few layers of silicon atoms, the electronic structure of the silicon that it describes is characteristic of the immediate vicinity of the silicon surface only and does not include band bending effects that occur over larger length scales within the silicon. Furthermore the bias voltages considered in the model are those between the region slightly below the silicon surface and the STM tip, whereas bias voltages measured experimentally are those between the STM tip and the deep silicon interior that is separated from the surface by regions where significant bias-dependent band bending occurs. Thus from the stand point of theory the applied bias will be characterized according to the location of the Fermi level of the tungsten tip (or, more precisely, its electrochemical potential) relative to the features of the carbon and silicon partial densities of states that are shown in Fig.5, rather than the numerical value of experimental bias voltage.

V. MODELING THE ELECTRONIC TRANSPORT

In the transport calculations reported here the electronic structures of the silicon substrate, molecules and tungsten tip are all treated together as a single system described by a single Hamiltonian. Thus, unlike in STM image calculations based on Bardeen tunneling theory, here the Hamiltonian matrix elements connecting orbitals of the molecules and those of the tip are *not* assumed to be small. Because of this the STM current can be calculated for small separations between the tip and molecules as well as large.

The calculations of the current are based on Landauer theory⁴⁴ which relates the electric current I through a nanostructure under an applied bias voltage V to the multichannel electron transmission probability $T(E, V)$ through the nanostructure at energy E as⁴⁵

$$I(V) = \frac{2e}{h} \int_{-\infty}^{\infty} dE T(E, V) (f(E, \mu_s) - f(E, \mu_d)) \quad (4)$$

where $f(E, \mu_i) = 1/(\exp[(E - \mu_i)/kT] + 1)$ and μ_i is the electrochemical potential of the source ($i = s$) or drain ($i = d$) electrode.⁴⁶

In the present work the source and drain electrodes are modelled as arrays of ideal leads: For calculations of vertical transport in the STM geometry, the electrode connected to the silicon substrate is modeled as an array of 152 ideal single-channel leads, one such lead coupled to the $1s$ orbital of each of the hydrogen atoms that passivate the silicon dangling bonds of the three lower layers of silicon atoms of the silicon cluster that represents the silicon substrate in Fig.3. The electrode connected to the STM tip was modelled as an array of 81 ideal single-channel tight-binding leads, one such lead coupled to each

of the 9 (s, p, d) valence orbitals of each atom of the model tungsten tip that is not the tip atom itself or one of its 5 closest neighbors. As well as mimicking macroscopic electrodes by supplying an ample electron flux to the system, this large number of ideal source and drain leads has a similar effect to phase-randomizing Büttiker probes⁴⁷ in minimizing the influence of dimensional resonances due to the finite sizes of the tungsten and silicon clusters employed in the model. Each ideal lead i was modelled as a semi-infinite tight-binding chain with a single orbital per site, a site energy α_i and nearest neighbor hopping matrix element β . α_i was chosen to be equal to the energy (including the shift, if any, due applied bias described in Section IV) of the hydrogen or tungsten orbital to which lead i was coupled. The hopping matrix elements β were all taken to have a magnitude of 5 eV, sufficiently large that the eigenmodes of all of the ideal leads in the energy window between μ_s and μ_d in eq. (4) be propagating.⁴⁶ The coupling matrix elements W_i between the ideal leads and their respective hydrogen and tungsten orbitals were also set equal to β .

To calculate $T(E, V)$ and hence evaluate eq.(4), the transformation to a different Hilbert space described in Refs. 48 and 49 was made, mapping the non-orthogonal basis of atomic orbitals discussed in Section IV to an orthogonal basis. The Lippmann-Schwinger equation

$$|\Psi_i\rangle = |\Phi_{o,i}\rangle + G_o(E)W|\Psi_i\rangle \quad (5)$$

describing electron scattering between the source and drain leads via the tungsten tip, molecules and hydrogen terminated silicon cluster was solved numerically for $|\Psi_i\rangle$ in the alternate Hilbert space.^{48,49} In eq.(5) $G_o(E)$ is the Green's function for the decoupled system (i.e., with the coupling between the ideal leads and the hydrogen and tungsten orbitals switched off), $|\Phi_{o,i}\rangle$ is the eigenstate of the decoupled ideal source lead i with energy E and $|\Psi_i\rangle$ is the corresponding scattering eigenstate of the complete system with the coupling W between the ideal leads and the hydrogen and tungsten orbitals switched on. The scattering amplitudes t_{ji} from the ideal source lead i to drain lead j at energy E were extracted from the scattering eigenstates $|\Psi_i\rangle$ and the transmission probability that enters eq. (4) was then calculated from

$$T(E, V) = \sum_i \sum_j \left| \frac{v_j}{v_i} \right| |t_{ji}|^2 \quad (6)$$

where v_i and v_j are the electron velocities in ideal leads i and j respectively at energy E .

Lateral transport through chains of styrene molecules on the silicon substrate was modelled similarly. However, in this case no STM tip was included in the model and no ideal leads were coupled to the silicon cluster or to the hydrogen atoms passivating it. Instead, 18 ideal single-channel leads representing a source electrode were coupled directly to the styrene molecule at one end of the styrene chain, one ideal lead coupling to each of the

atomic valence p-orbitals of each carbon atom of the benzene ring of the molecule. 18 ideal single-channel leads representing the drain electrode were coupled similarly to the styrene molecule at the other end of the molecular chain. In this case transport through the styrene chains via bands derived from molecular HOMO and LUMO orbitals was being investigated so the site energies α_i of the orbitals making up the ideal leads were chosen lying within the molecular HOMO and LUMO energy bands, respectively. The nearest neighbor hopping matrix element β of the ideal leads was chosen so that the widths of the energy bands of the ideal leads were comparable to the widths of the energy bands derived from the molecular HOMO and LUMO energy levels.

VI. RESULTS: VERTICAL TRANSPORT IN THE STM GEOMETRY

A. Negative sample bias

Fig. 6 shows representative results for the calculated current flowing between the tungsten STM tip and the styrene/methyl-styrene molecular chain on silicon that is depicted in Fig.3. The silicon substrate is biased negatively with respect to the STM tip so that occupied states of the molecular chain and substrate are being probed. Each curve corresponds to a scan of the STM tip along the line of molecules at a constant height above the silicon substrate.⁵⁰ The lateral position of the highest carbon atom of each molecule is indicated by a dotted vertical line labelled m (methyl-styrene) or s (styrene). Curves L and L' correspond to a low value of the bias such that the Fermi level of the tungsten tip is at -12.0 eV as indicated by the arrows labelled L in Fig.5 (b) and (c). Since in this case the tungsten Fermi level is well above the upper edge of the molecular HOMO band in Fig.5 the current is due to electron *tunneling* through the molecules from the silicon substrate states to the STM tip. Curve H is for a higher bias with the tip Fermi level at -12.6 eV as indicated by the arrow labelled H in Fig.5(b). In this case the tungsten Fermi level is within of the molecular HOMO band that is located on the molecular benzene rings and mediates transport between the silicon substrate and the tip. For curves L and H the tungsten atom at the end of the tip is at a height 2 Å higher than the highest carbon atom of the molecular chain while for curve L' the tip atom is 3 Å higher than the highest carbon atom. (Note that for curve H the current shown has been scaled down by a factor of 10 for clarity).

Curve L is similar to experimental scans along the molecular chain at low negative sample bias (Fig.2 (a) and (b)), although the experimental scans were taken at constant current while the calculation was performed at constant tip height.⁵² In curve L each molecule appears as a distinct current *maximum* consistent with the experimental data,⁵³ and the local current over each styrene molecule is somewhat stronger than over

a methyl-styrene molecule (as in Fig.2 (a)) despite the fact that the methyl-styrene molecule is the taller of the two.⁵⁴ Interestingly, as the tip is raised higher above the molecular chain at constant (low) bias the current flowing through the styrene molecules is predicted to decrease initially much faster than that through the methyl-styrene, resulting in the significantly weaker styrene current seen for curve L'. We attribute this to different behavior of weak transport resonances (involving both tip states and carbon-silicon interface states) for the styrene molecule than for the methyl-styrene molecule that is much closer to the tip and thus interacts more strongly with it.⁵⁵

As the bias increases, the calculated current through the methyl-styrene molecules increases more rapidly than through the styrene and the relative amplitude of the current corrugation along the molecular chain decreases along both the styrene and methyl-styrene parts of the chain. Both of these effects (that are clearly visible in curve H) are also seen experimentally in Fig.2 (a) and (b).⁵⁵

The above theoretical results imply that the observation of an experimental STM profile similar to L in Fig. 6 signals that the STM tip Fermi level lies between the Si valence band edge at the Si surface and the HOMO band of the molecular chain, whereas the observation of a profile similar to H signals that the tip Fermi level lies below the upper edge of the HOMO band. Since a transition from an L type profile to a H type profile is in fact observed experimentally as the magnitude of the substrate bias is increased (see Fig. 2), our experimental and theoretical findings taken together confirm that the molecular HOMO band does in fact lie significantly below the silicon valence band edge, as we have already suggested in Section IV based on the nature of the corrugation observed along the molecular chain at low negative substrate bias.

Another interesting aspect of the results shown in Fig. 6 occurs at the junction of the methyl-styrene and styrene chains: At low bias (curves L and L') the current profile of the styrene molecule at the junction is quite similar to those of the styrene molecules far from the junction, and the same is true of the methyl-styrene molecules. However, this is *not* true at high bias (curve H) where the current decreases *monotonically* from the methyl-styrene side of the junction all the way through the location of the first molecule on the styrene side; the first styrene molecule is not visible as a distinct entity, in marked contrast to what is seen near the junction in curve L'. We attribute this smearing of the boundary between the methyl-styrene and styrene chains in the STM image at high bias to delocalization of electron states along the molecular chain associated with overlapping molecular HOMO levels on adjacent molecules. This effect is not found in the STM images at low bias (curves L and L') where the states outside of the molecular HOMO band are responsible for conduction. We will return to this topic in our discussion of positive sample bias below and its relation to lateral transport along the molecular chain

will be considered at the end of Section VII.

Increased smearing of the boundary between the methyl-styrene and styrene chains with increasing bias is also seen in the experimental STM data in Fig.2 (a) and (b). However, experimentally the apparent height of the molecular chain varies on both sides of the junction but more so on the methyl-styrene side. The reason for this difference between theory and experiment is unclear at the present time.

The calculated current peaks for STM tip scans at low bias and constant height in the direction orthogonal to that of the scans in Fig. 6 exhibit internal structure. This can be seen in Fig.7(a) where curve sL (mL) is the result of such a scan across the third styrene (methyl-styrene) molecule from the junction for the same bias and tip height as scan L in Fig.6. With increasing bias voltage the internal structure becomes less prominent and the scans evolve to a simpler single-peak structure.

B. Positive sample bias

Fig. 8 shows the calculated current between the STM tip and the molecular chain for some values of positive substrate bias. The tip is scanned along the molecular chain at constant height,⁵⁰ 2 Å higher than the highest carbon atom in each case. The silicon substrate is biased positively with respect to the STM tip so that unoccupied states of the molecular chain and substrate are being probed. Dotted vertical lines again indicate positions of the highest carbon atoms of the styrene (s) and methyl-styrene molecules. The tungsten Fermi level is located below the molecular LUMO band for curves ll and l, slightly above the lower edge of the LUMO band for curve e, and well inside the LUMO band for curve h, at -9.3 eV, -8.6 eV, -8.39 eV and -8.2 eV respectively, as is indicated by arrows in Fig. 5(b). At low positive bias (curves ll and l) electrons tunnel from the tungsten tip to the silicon substrate states through the molecules *outside* of the energy range of the molecular LUMO band and the current shows a peak over each molecule, as for the case of low negative substrate bias (curves L and L' of Fig. 6). As the bias increases and the tungsten Fermi level begins to enter the molecular LUMO band, the current develops a minimum over the center of each styrene molecule because the molecular LUMO has π -like character with a wave function node in the plane of the benzene ring.⁵⁶ A similar effect also happens over the methyl-styrene molecules with increasing bias, but more slowly because of the presence of the methyl group between the benzene ring and the STM tip: The amplitude of the current corrugation over the methyl-styrene chain decreases from curve ll to curve e and then reverses so that for curve h the current is depressed over the center of each molecule. The amplitude of the current corrugation also decreases with increasing bias (from curve e to curve h) over the styrene chain. At low bias the contrast between the methyl-styrene and styrene decreases with

decreasing bias (from curve l to curve ll) but does not reverse as in Fig.6.

Interestingly, the current for curve e develops a strong overall slope from molecule to molecule extending across the *entire* styrene chain, an effect that is not found for curves ll, l and h or under negative substrate bias (Fig. 6). There is also a weaker slope across the methylstyrene chain. This suggests that electronic communication between the molecules over a length of several inter-molecular spacings is important at this bias voltage and strongly affects the calculated STM image of the molecular chain. This will be explored further in Section VII.

Fig.7(b) shows the calculated tip current for scans across the molecular chain at positive substrate bias in the direction orthogonal to the scans in Fig. 8. Curve se (me) is the result of such a scan across the third styrene (methylstyrene) molecule from the junction for the same bias and tip height as scan e in Fig.8. Note the double peaked structure in scan se. This double peaked structure over styrene evolves into a single peak with increasing and decreasing bias, while the scan across methylstyrene remains single-peaked.

VII. LATERAL TRANSPORT AND ITS INFLUENCE ON STM IMAGES

The overlaps between the molecular HOMO and LUMO states of adjacent styrene and methylstyrene molecules in the molecular chains on silicon have the potential to give rise to bands of electronic states delocalized along the molecular chains.^{9,10} However, the molecular LUMO (HOMO) energy levels are degenerate with states of the silicon conduction (valence) band and clearly must hybridize with them to some degree. Moreover these molecular energy levels correspond to excited states of the total system and electrons (holes) occupying them must eventually decay to lower energy conduction (valence) states of the substrate due to inelastic processes. However, it is still interesting from a theoretical perspective to determine how much the hybridization between a molecular chain's LUMO and HOMO bands and the silicon conduction and valence bands affects electron or hole transport along short stretches of the molecular chains. For example, if an electron (hole) is injected into the LUMO (HOMO) orbital of a molecule belonging to the chain and extracted by a probe at another site along the molecular chain, is the transport between the two sites dominated by conduction through the molecular chain or through the substrate or do these two conduction channels make comparable contributions to the transport? A related quantity, the characteristic distance that an electron or hole injected into a LUMO or HOMO state of the molecular chain from an STM tip travels along the chain before being absorbed into the silicon substrate, may influence the STM image of a molecular chain, particularly near a heterojunction. In this Section

the issue of parallel transport along the molecular chain and through silicon substrate over nanoscale distances is addressed theoretically, and the results are related qualitatively to the findings regarding the calculated STM images of the molecular chains that were presented in Section VI.

The approach used is to calculate the multichannel Landauer transmission probabilities for electrons between a pair of ideal electrodes coupled to the ends of a molecular chain of 8 styrene molecules on a dimerized hydrogen-terminated silicon substrate. For the calculations presented here 9 layers of silicon atoms were included in the cluster modeling the silicon substrate. However, results obtained with a 5 silicon layer model of the cluster were similar. The ideal source and drain electrodes were coupled to the benzene rings of the molecules at the two ends of the styrene chain and were represented by arrays of ideal single channel leads as described at the end of Section V. The energy bands of the ideal leads were taken to be centered at $\alpha_i = -12.7$ eV (-8.25 eV) for studies of the lateral transport in the energy range of the molecular HOMO (LUMO) band; the ideal lead hopping parameter β was chosen to be -0.25 eV for an ideal lead band width of 1 eV. The hamiltonian matrix elements coupling the ideal leads to the carbon p-orbitals of the molecular benzene rings was chosen to be 0.4β .

The calculated Landauer transmission probability $T(E)$ (per spin channel) through the system for energies corresponding to the LUMO band of the styrene chain is shown in Fig. 9(a). These results show that the system is a fairly good one-dimensional conductor with at least two partially-transmitting channels per spin in the energy range around the middle of the LUMO band since $1 \lesssim T < 2$ through much of this energy range.

To determine whether this strong transmission is occurring mainly by direct electron transmission from molecule to molecule along the chain or mainly through the silicon substrate the calculation was repeated with all Hamiltonian matrix elements and overlaps between atomic orbitals on different molecules switched off so as to allow conduction along the chain to proceed only via the substrate. (Note that the parameters describing the ideal leads and their coupling to the sample were kept unchanged.) The result is shown in Fig.9(b). Clearly throughout most of the LUMO energy band the transmission via the substrate channel (Fig.9(b)) is much weaker than the direct transmission through the molecular chain itself. The transmission through the substrate is strong only at a small number of narrow resonances. Furthermore at the energies at which the strongest of these resonances occur the transmission of the fully coupled system (Fig.9(a)) shows *minima*; this means that the resonant states of the substrate that give rise to the strongest transmission peaks in Fig.9(b) give rise to resonant *back-scattering* (as opposed to contributing to resonant forward transmission) in the fully coupled system where transport is permitted through both the molecular chain and substrate. Thus it is quite clear that in the energy

range of the LUMO band of the molecular chain, transport from one end of the molecular chain to the other is strongly dominated by direct electron transmission from molecule to molecule.⁵⁸

The corresponding results for transmission from one end of the molecular chain to the other in the energy range of the molecular HOMO band are shown in Fig.9(c) for the fully coupled system, and in Fig.9(d) for the system with all Hamiltonian matrix elements and overlaps between atomic orbitals on different molecules switched off. The molecular chain is still a fairly good one-dimensional conductor ($T(E) \sim 1$ in most of this energy range in Fig.9(c)). Transmission through the substrate (Fig.9(d)) is again clearly less efficient than through the molecular chain although the difference between the two is much less stark for the HOMO energy range than for the LUMO.

A simple measure of the overall relative importance of direct transmission from molecule to molecule along the molecular chain relative to that via the parallel path through the substrate is the ratio R of the average transmission for the fully coupled system to the average transmission with the molecule-to-molecule coupling switched off. For the 8 styrene molecule chain $R \sim 30$ for the molecular LUMO band while for the molecular HOMO band $R \sim 4$.

For ideal source and drain leads coupled to opposite ends of the substrate instead of to the molecular benzene rings at the ends of the styrene chain, the calculated average transmission probabilities in the HOMO and LUMO energy ranges were found to be similar in magnitude. Thus the above difference in R between the HOMO and LUMO bands of the molecular chain is mainly due to weaker hybridization of the substrate orbitals with the molecular LUMO states and than with the molecular HOMO.

Since the above calculations indicate that states of the LUMO band of the molecular chain hybridize much less with the states of the silicon substrate than the states of the molecular HOMO band do, it is reasonable to expect it to be easier for STM measurements to detect a distinctive signature of electronic states confined to the molecular chain and extending over a significant distance along the molecular chain in the LUMO energy range than in the HOMO range. The results of the calculations of vertical transport in the STM geometry presented in Section VI are consistent with this: In particular, one of the theoretical STM current plots (curve e) in Fig. 8 shows an overall decline in the STM current as one moves away from the center of the molecular chain in either direction; the decline extends all the way to the end of the molecular chain in either direction but is especially strong on the styrene side of the chain. At the bias voltage corresponding to this current plot, the Fermi level of the STM tip is slightly above the lower edge of the LUMO band of the molecular chain and a single transmission resonance due to lowest electronic eigenstate belonging to the LUMO band makes the dominant contribution to

the current. The electron probability distribution in this eigenstate is peaked at the center of the molecular chain and declines strongly towards both ends of the molecular chain. This explains qualitatively why the calculated STM current (curve e, Fig. 8) is stronger at the center of the chain than at its ends. (However, to predict the current profile along the chain *quantitatively* knowledge of the LUMO eigenfunction alone is not sufficient and a complete transport calculation such as is described in Section V is necessary.) By contrast, the calculated STM current for the case where the HOMO band of the molecular chain is being probed does not show such pronounced trends across more than a single molecule, even when the tungsten Fermi level is close to the edge of the HOMO band, just as one might expect qualitatively for a molecular band that mixes more freely with states belonging to the substrate.

VIII. END EFFECTS

The model geometries of the molecular chains studied theoretically in the preceding sections were constructed (see Section III) to be representative of regions of the chain far from its ends. This was done by constraining the average spacing between the tops of the molecules to be similar to that observed experimentally near the center of the molecular chain. If this constraint is *not* imposed, molecules at the ends of the chain tilt more strongly towards the silicon substrate. This is seen experimentally in Fig. 2(a) and (b), where the apparent difference in height between the end and central molecules of the chain at low negative sample bias is more than an Angstrom. However, the observed height contrast between the ends and center of the chain in Fig. 2(a) and (b) decreases markedly as the magnitude of the bias increases. Thus considerations other than the geometrical height profile of the molecular chain must also be taken into account to explain this data.

The gaps between the molecular HOMO and LUMO bands of stacks of parallel-oriented aromatic molecules should increase with increasing separation between the molecules because the coupling between adjacent molecules decreases as their separation increases.¹⁵ This suggests the following scenario as a simple explanation of the bias-dependence of the STM profiles of the molecular chains that we have observed: The tilting apart of the molecules near the ends of the chains causes the local HOMO-LUMO band gap of the molecular chain to increase towards the ends of the chain. In constant current STM images at low bias where the Fermi level of the tip is in the molecular HOMO-LUMO band gap, this increased band gap causes the molecular chain to appear *lower* at its ends relative to its center than the geometrical difference in height alone would require. At larger bias, when the tip Fermi level has fallen below the (local) top of the molecular HOMO band throughout the molecular chain and *all* of the molecules have “turned on,”

the end molecules appear less diminished. It appears therefore that the variable HOMO-LUMO gap scenario could account qualitatively for the position and voltage dependent height variations observed. However, a more thorough analysis shows this model to be incomplete; it does not take into account three aspects of this system that we show below to be crucial. They are: (1) The molecules bond to equally spaced Si dimers on the (001) silicon surface. Thus although the spacing of the tops of the molecules in STM images varies along the chain due to the varying tilt of the molecules from the surface normal, the spacing between the bottoms of the molecules is fixed and thus, as will be seen below, even the most strongly tilted molecule at the end of the chain couples strongly to the rest of the chain. (2) The coupling of molecular HOMO and LUMO orbitals to the substrate (to which vertical transport is very sensitive) increases strongly along the chain as its end is approached because of the increasing tilt of the molecules towards the substrate.⁵¹ (3) At low bias where the STM tip Fermi level is in the molecular HOMO-LUMO gap the transmission of electrons between the substrate and tip is mediated by resonant states at the C-Si interface rather than the molecular HOMO and LUMO orbitals, as is discussed in Section VI; i.e., a different transport mechanism that is not included in the pure variable band gap scenario outlined above operates in the low bias regime.

For simplicity, we restrict our attention to styrene chains. Our results for the (vertical) STM current over a chain of 8 styrene molecules on a hydrogen-terminated dimerized Si(100) substrate for negative sample bias are shown in Fig. 10. The silicon substrate, tungsten STM tip and ideal source and drain leads are as in Section VI. However, the structure of the molecular chain is different: Here the final AM1 relaxation of the chain differed from that described in Section III in that the styrene molecule at the left end of the chain was constrained to stand upright on the substrate (with a small tilt to the right) but the other molecules were not constrained in this way. Thus the structure of this model styrene chain near its left end resembles that in the interior of long molecular chain (as for the model structures considered in Section VI) while its right end should be similar to that of the real end of a molecular chain. The currents shown in Fig. 10 are calculated for STM tip trajectories that pass directly over the 4th carbon atom of the benzene ring of each styrene molecule, i.e., the carbon atom furthest from the carbon chain that anchors the benzene ring to the silicon. [The locations of these carbon atoms are shown by dotted vertical lines in Fig. 10.] This 4th carbon atom for the molecule at the right end of the model styrene chain is located 1.12 Å closer to the Si substrate than the highest carbon atom of the chain,^{59,60} a height difference similar to the apparent height contrast between the end and interior molecules of the chain observed experimentally at low bias; see Fig. 2(a,b). The current plots L (H) in Fig. 10 are for the same low (high) values of the negative sample bias as the plots L (H) in Fig. 6; for L (H)

the STM tip Fermi level is above (within) the molecular HOMO band as in Fig. 5. However, in Fig. 10 the currents labelled H have been scaled up by a factor of 5 for clarity while that in Fig. 6 was scaled down by a factor of 10. The solid curves L and H in Fig. 10 show the calculated STM current for scans at constant tip height above the Si substrate (the same height as for curves L and H in Fig. 6). The dashed curves, however, show calculated currents for tip trajectories which follow the sloping height profile of the relaxed molecular chain (thus at varying height from the underlying silicon surface).⁶¹

For the scans at constant height above the silicon surface (the solid curves) the calculated current over the tilted molecule at the right end of the chain is lower than that near the left end, by a factor of more than 30 for the low bias case L and a factor of ~ 10 for the higher bias case H. These results agree qualitatively with our experimental finding that the height of the molecules appears lower at the end of the chain and that the magnitude of the lowering decreases as the magnitude of the bias increases. However for the lower bias scan at a constant vertical distance above the tops of the molecules (dashed curve L) the calculated current does not decrease near the right end of the molecular chain; in fact it is slightly *higher* over the molecule that ends the chain than over the rest of the chain. By contrast, for the simple position-dependent band gap model outlined above to apply in isolation the apparent height of the molecules at the end of the chain *must* be substantially *lower* than their geometrical height. Thus our calculations do not support a purely position-dependent band gap scenario. They suggest instead that at low negative substrate bias in the constant current STM mode the experimentally measured differences in the height of the tip from styrene molecule to styrene molecule along the chain should, to a first approximation, be equal to the differences in the geometrical heights of the tops of the respective molecules. This interpretation is further supported by the approximate agreement between the apparent height difference in experimental data in Fig. 2(a,b) between the styrene molecules near the center and end of the chain at low bias and the result of our calculation of the structure at the end of the molecular chain: In each case the top of the molecule at the end of the chain is lower than the tops of the molecules far from the ends by somewhat more than 1 Å.

We explain the bias dependence of the apparent height of the molecules at the end of the chain relative to those far from the end as follows: Because the molecules near the end of the chain tilt more strongly towards the substrate than the other molecules of the chain do, the molecular HOMO orbitals of the end molecules (being mainly on the benzene rings) couple much more strongly to the substrate than the HOMO orbitals of the other molecules do. This stronger coupling leads to stronger electron transmission from the substrate to the STM tip through the end molecules of the chain than through the other molecules at the higher values of the negative

substrate bias for which the Fermi level of the tungsten tip falls below the top of the molecular HOMO band so that transport via the HOMO orbitals dominates the conduction.⁶³ Thus for the dashed curve H in Fig. 10 where the tip scans along the chain at same vertical distance above each molecule, the current grows quite significantly as the end of the chain is approached. Consequently the decrease in the apparent height of the molecules as the end of the chain is approached in *constant current* STM mode is not as strong as it is at lower bias where the molecular HOMO states do not mediate the transport.⁶³

This mechanism is clarified further by the inset of Fig. 10: Here the Landauer transmission $T(E, V)$ between the substrate and STM tip is plotted as a function of electron energy E for the same (higher) value of the applied bias V as for curves H of Fig. 10. For each transmission curve plotted the STM tip is located 3.497 Å above the 4th carbon atom of the benzene ring of the nearest molecule (as for the dashed curve H of Fig. 10). For reference the arrow indicates the HOMO energy of an ethyl-benzene molecule in free space. The solid line is the calculated transmission with the tip above the molecule at the right end of the molecular chain (with the other molecules of the chain also present on the substrate). The dashed line shows the transmission with the tip above the same molecule (with the same tilted geometry) but with the other molecules of the chain removed from the system and replaced by hydrogen atoms. The dot-dashed curve is the average transmission for tip positions over the 5 molecules closest to the left end of the molecular chain. The nearly equally spaced peaks of the dot-dashed curve arise from states of the molecular HOMO band that is formed due to the coupling between the HOMO orbitals of the molecules making up the chain.⁶⁴ The much greater strength of the transmission for the tip above the molecule at the right end of the chain (solid curve) is due to the stronger coupling of that molecule's HOMO orbital to the substrate, as discussed above. It results in the stronger current when the tip is over the right end molecule than over the rest of the chain, as is seen in the dashed curve H. The stronger coupling of the right end molecule's HOMO to the substrate also results in the strong broadening of the the associated transmission peaks (solid and dashed lines of the inset); the HOMO transmission peaks (not shown) for isolated molecules on the substrate with the upright geometries of molecules far from the end of the chain are much narrower, with widths similar to those of the individual peaks of the dot-dashed curve of the inset.

Although, as we have shown, the enhanced coupling of the molecular HOMO at the end of the chain to the substrate plays a crucial role in the bias dependence of the STM profile of the end of the chain, the coupling of the end molecule to the rest of the molecular chain remains strong despite the tilting of the end molecule towards the substrate. This is evident from a comparison of the transmission peaks for the end molecule with the

rest of the molecular chain present and absent from the system: The coupling of the end molecule to the rest of the chain results in the large splitting of the transmission peak that occurs when the rest of the molecular chain is present (solid curve of the inset) and does not occur when the rest of the chain is absent (dashed curve).^{65,66}

Our results for positive substrate bias are shown in Fig. 11. The chain geometry and the meaning of the solid and dashed plots are as in the negative bias case (Fig. 10). As in Fig. 8, for plots l, e and h the STM tip Fermi level is below, slightly above and well above the lower edge of the molecular chain's LUMO band (see Fig. 5), but in Fig. 11 the currents l have been scaled down by a factor of 10. The molecules at the end of the chain are again predicted to appear lower in STM images than those near the center, and this lowering becomes less pronounced as the magnitude of the applied bias voltage increases.⁶⁷ The mechanism of the bias dependence is similar to that for negative substrate bias: Because of the tilting of the molecules at the end of the chain, their LUMO orbitals couple more strongly to the substrate, and this results in stronger and broader transmission peaks (and an enhanced STM current) over the end molecules when the applied bias is large enough for the LUMO orbitals to participate in conduction. However, for plots e and h of Fig. 11 the local current *maxima* occur over or near the tops of the molecules near the end of the chain while far from the end current *minima* coincide with the molecular positions. Because of the long distance that the influence of the physical (right) end of the molecular chain extends along the chain in plot e, experimentally distinguishing effects related to the presence of a heterojunction from such end effects in empty-state STM imaging will require long molecular chains and careful analysis.

IX. CONCLUSIONS

We have synthesized heterojunctions of lines of styrene and methyl-styrene molecules on H-terminated (100) silicon substrates and have studied these systems with scanning tunneling microscopy as well as theoretically. We have developed a tight binding theory based on the extended Hückel model (modified so as to provide a good description of the electronic structure of tungsten and silicon crystals as well as of the molecules) that together with Green's function and Landauer transport techniques is able to account for key features of the experimental filled-state STM images of these molecular systems (including both the heterojunctions and the regions near the ends of the molecular chains) and of their variation with applied bias voltage. This model has also been used to explore theoretically the lateral transport properties of short chains of styrene molecules on silicon and it has been found that electron transmission along such chains should occur primarily from molecule to molecule rather than through the parallel substrate channel, especially in the energy range of the molecular LUMO band. The

calculations also suggest that phenomena due to electron wave functions extending from molecule to molecule (such as states localized around the heterojunction of a pair of molecular wires) may be observable experimentally by STM imaging.

Acknowledgments

This research was supported by the Canadian Institute for Advanced Research, NSERC, iCORE and the NRC.

We have benefited from discussions with G. DiLabio and J. Pitters and from the technical expertise of D.J. Mofatt, and M. Cloutier.

- ¹ L. A. Bumm, J. J. Arnold, M. T. Cygan, T. D. Dunbar, T. P. Burgin, L. Jones II, D. L. Allara, J. M. Tour, and P. S. Weiss, *Science* **271**, 1705 (1996).
- ² M. A. Reed, C. Zhou, C. J. Muller, T. P. Burgin, and J. M. Tour, *Science* **278**, 252 (1997).
- ³ S. Datta, W. Tian, S. Hong, R. Reifenberger, J. I. Henderson, C. P. Kubiak, *Phys. Rev. Lett.* **79**, 2530 (1997).
- ⁴ J. Chen, M. A. Reed, A. M. Rawlett and J. M. Tour, *Science* **286**, 1550 (1999).
- ⁵ C. P. Collier, G. Mattersteig, E. W. Wong, Y. Luo, K. Beverly, J. Sampaio, F. M. Raymo, J. F. Stoddart and J. R. Heath, *Science* **289**, 1172 (2000).
- ⁶ Z. J. Donhauser, B. A. Mantooth, K. F. Kelly, L. A. Bumm, J. D. Monnell, J. J. Stapelton, D. W. Prince Jr., A. M. Rawlett, D. L. Allara, J. M. Tour and P. S. Weiss, *Science* **292**, 2303 (2001).
- ⁷ For a review see R. A. Wolkow, *Annu. Rev. Phys. Chem.* **50**, 413 (1999).
- ⁸ G. P. Lopinski, D.D.M. Wayner, R.A. Wolkow, *Nature* **406**, 48 (2000).
- ⁹ J.-H. Cho, D.-H. Oh, and L. Kleinman, *Phys. Rev. B* **65**, 081310(R) (2002).
- ¹⁰ W. A. Hofer, A. J. Fisher, G. P. Lopinski, R. A. Wolkow, *Chem. Phys. Lett.* **365**, 129 (2002).
- ¹¹ N. P. Guisinger, M. E. Greene, R. Basu, A. S. Baluch, and M. C. Hersam, *Nano Letters* **4**, 55 (2004).
- ¹² X. Tong, G. A. DiLabio, R. A. Wolkow, *Nano Letters* **4**, 979 (2004).
- ¹³ T. Rakshit, G.-C. Liang, A. W. Ghosh, and S. Datta, *Nano Letters* **4**, 1803 (2004).
- ¹⁴ Y. Wang and G. S. Huiyang, *Appl. Phys. Lett.* **86**, 023108 (2005).
- ¹⁵ A. Rochefort, R. Martel and P. Avouris, *Nano Letters* **2**, 877 (2002).
- ¹⁶ S. N. Yaliraki and M. A. Ratner, *J. Chem. Phys.* **109**, 5036 (1998).
- ¹⁷ M. Magoga and C. Joachim, *Phys. Rev. B* **59**, 16011 (1999).
- ¹⁸ N. D. Lang and P. Avouris, *Phys. Rev. B* **62**, 7325 (2000).
- ¹⁹ J. G. Kushmerick, J. Naciri, J. C. Yang, and R. Shashidhar, *Nano Lett.* **3**, 897 (2003).
- ²⁰ R. Liu, S.-H. Ke, H. U. Baranger, and W. Yang, *J. Chem. Phys.* **122**, 044703 (2005).
- ²¹ J. J. Boland, *Surf. Sci.* **261**, 17 (1992).
- ²² Submitted. Also G.A. DiLabio, *et al.* *J. Am. Chem. Soc.* **126**, 16048 (2004) for examples of the self-directed growth of linear alkane molecules.
- ²³ Other methyl-styrene/styrene heterostructures have been studied (not shown) which still possess the terminal silicon radical. They image with similar characteristics but show locally perturbed electronic structure at low magnitude bias resulting from interaction with the terminal silicon radical.²⁴ Empty-state images (not shown) were successfully acquired for a single heterostructure, and will not be discussed.
- ²⁴ P.G. Piva, G.A. DiLabio, J.L. Pitters, J. Zikovsky, M. Rezek, S. Dogel, W.A. Hofer, R.A. Wolkow, *Nature* **435**, 658 (2005).
- ²⁵ The conformation of the styrene and methyl-styrene molecules depicted in Fig.3 and studied theoretically in this article is based on the bonding geometry of chains of styrene molecules to the H-terminated Si (100) surface adopted in a number of previous studies of those systems.^{8,10,14} However, a subtly different structure for the styrene chains on silicon may also be possible. In this alternate structure,^{9,26} the carbon atom adjacent to the carbon atom that bonds to the silicon is located not above the trench between the silicon dimer rows as in Fig.3 but above the silicon dimer to which the molecule bonds.⁹ However the benzene ring of the molecule is still located over the trench between the dimer rows. Which geometry is realized in practice remains unclear: Density functional calculations are not reliable enough to decide unequivocally which geometry has the lower energy, and it is not known whether either structure is favored over the other by growth kinetics of the molecular rows. Comparison of STM images of the styrene/methyl-styrene heterojunctions with the results of our modeling also does not unambiguously favor one of these geometries over the other.
- ²⁶ G.A. DiLabio, private communication.
- ²⁷ The Gaussian98 package with the B3LYP density functional and 6-31G(d) basis set were used.
- ²⁸ The AM1 relaxations were carried out using the Gaussian98 package.
- ²⁹ The identification between the spacing of the molecules as measured in the experimental STM images and the lateral spacing of the top carbon atoms of the molecules is justified by our calculations of the STM current maps at low bias as discussed in Section VIA.
- ³⁰ The Gaussian98 package with the B3PW91 density functional and Lanl2DZ basis set was used.
- ³¹ E. G. Emberly, G. Kirczenow, *Phys. Rev. B* **58**, 10911 (1998); S. N. Yaliraki, M. Kemp, M. A. Ratner, *J. Am. Chem. Soc.* **121**, 3428 (1999); V. Mujica, A. E. Roitberg, M. Ratner, *J. Chem. Phys.* **112**, 6834 (2000); L.

- E. Hall, J. R. Reimers, N. S. Hush and K. Silverbrook, J. Chem. Phys. **112**, 1510 (2000); M. Di Ventura, S. T. Pantelides, and N. D. Lang, Phys. Rev. Lett. **84**, 979 (2000); P. S. Damle, A. W. Ghosh and S. Datta, Phys. Rev. B **64**, 201403 (R) (2001); J. Taylor, H. Guo, J. Wang, Phys. Rev. B **63**, 121104 (R) (2001); P. E. Kornilovitch and A. M. Bratkovsky, Phys. Rev. B **64**, 195413 (2001).
- ³² E. G. Emberly and G. Kirczenow, Phys. Rev. Lett. **87**, 269701 (2001), Phys. Rev. B **64**, 235412 (2001).
- ³³ M. Paulsson, S. Stafstrom, Phys. Rev. B **64**, 35416 (2001); J. J. Palacios, A. J. Pérez-Jiménez, E. Louis, J. A. Vergés, Phys. Rev. B **64**, 115411 (2001); M. H. Hettler, H. Schoeller, W. Wenzel, Europhys. Lett. **57**, 571 (2002); J. Taylor, M. Brandbyge, K. Stokbro, Phys. Rev. Lett. **89**, 138301 (2002); J. Heurich, J. C. Cuevas, W. Wenzel, G. Schön, Phys. Rev. Lett. **88**, 256803 (2002); R. Gutierrez, F. Grossmann, R. Schmidt, Chemphyschem **3**, 650 (2002).
- ³⁴ J. G. Kushmerick, D. B. Holt, J. C. Yang, J. Naciri, M. H. Moore, R. Shashidhar, Phys. Rev. Lett. **89**, 086802 (2002).
- ³⁵ E. G. Emberly and G. Kirczenow, Phys. Rev. Lett. **91**, 188301 (2003); Y. Xue and M.A. Ratner, Phys. Rev. B **69**, 085403 (2004), Phys. Rev. B **70**, 081404 (2004); S.H. Ke, H.U. Baranger, W.T. Yang **70**, 085410 (2004).
- ³⁶ C.C. Kaun, H. Guo, Nano Letters **3**, 1521 (2003).
- ³⁷ T. Lee, W. Wang, J. Klemic, J. Zhang, J. Su, and M. A. Reed, J. Phys. Chem. B **108**, 8742 (2004).
- ³⁸ These difficulties may be related in part to the fact that while Kohn-Sham theory is appropriate for calculating total energies and relaxed molecular geometries, the single-electron eigenenergies and wave functions that appear in it do not have a rigorous physical meaning.³⁹ While they are often used successfully to approximate the corresponding properties of electronic quasi-particles that play a crucial role in transport, this approximation need not be accurate in general.
- ³⁹ W. Kohn and L.J. Sham, Phys. Rev. **140**, A1133 (1965).
- ⁴⁰ Seven independent fitting parameters K_{ij} with values falling in the range between 1.0 and 2.0 were found to suffice for this purpose.
- ⁴¹ The tungsten Hamiltonian matrix elements were fitted to the band structure of bulk bcc tungsten given by D.A. Papaconstantopoulos, in *Handbook of the Band Structure of Elemental Solids*, Plenum Press, New York, 1986. The Fermi level of the model tungsten STM tip at zero bias was set 0.45 eV below the calculated HOMO level of the 15 atom tungsten cluster used to model the tip to improve the match between features of the density of states of the model tip and those of bulk tungsten around the Fermi level.
- ⁴² E. G. Emberly, G. Kirczenow, Chem. Phys. **281**, 311 (2002), Appendix A.
- ⁴³ In reality a part of the potential drop should occur within the molecule and it has been proposed that this may result in negative differential resistance (NDR) in STM experiments involving molecules on silicon.^{11,13} Since NDR has not been observed experimentally in the styrene and methyl-styrene molecular chains on silicon in this and previous⁸ work, it seems reasonable to neglect the bias-induced potential drop across the molecules, as a first approximation, for the bias voltages considered here.
- ⁴⁴ For a review see S. Datta, *Electronic Transport in Mesoscopic Systems*, Cambridge University Press: Cambridge, 1995.
- ⁴⁵ The applied bias shifts the energy levels of the STM tip relative to those of the Si substrate and molecules. Since we use a realistic tight-binding model to describe the tungsten STM tip, this relative shift of the energy levels results in the transmission coefficient $T(E, V)$ depending on the value of the applied bias V as well as on the electronic energy E .
- ⁴⁶ The temperature T in the Fermi functions was set to 0 in the calculations reported here.
- ⁴⁷ M. Büttiker, Phys. Rev. B **33**, 3020 (1986).
- ⁴⁸ E. Emberly and G. Kirczenow, Phys. Rev. Lett. **81**, 5205 (1998).
- ⁴⁹ E. G. Emberly and G. Kirczenow, J. Phys.: Condens. Matter **11**, 6911 (1999).
- ⁵⁰ The trajectory of the tip is above approximately the centerline of the “trench” between the two rows of Si dimers in Fig.3.
- ⁵¹ An analogous effect has been proposed for aromatic molecules on metal substrates by P. E. Kornilovitch and A. M. Bratkovsky, Phys. Rev. B **64**, 195413 (2001).
- ⁵² Since the STM current at constant bias is a decreasing function of tip height, regions of higher current at constant tip height coincide with regions of greater tip height at constant current.
- ⁵³ The current node predicted to occur at the center of each molecule at low bias by density functional theory is absent in both the present theoretical results and the corresponding experimental data.
- ⁵⁴ The fact that curve L of Fig.6 for which the tip is only 2 Å higher than the highest carbon atom of the molecular chain resembles the experimental data at low bias closely (whereas curve L' for which the tip is 1 Å higher than than for curve L does not) underscores the importance of modeling the present system without treating the electronic Hamiltonian matrix elements and overlaps between the tip and molecules as weak perturbations, as is frequently done in theories of STM imaging. The present theoretical approach avoids making such a weak coupling approximation as is explained at the start of Section V.
- ⁵⁵ In an alternate model of the STM tip in which the tungsten atom at the end of the tip is replaced by a silicon atom, the calculated STM current was also found to exhibit a decreasing contrast between the methyl-styrene and styrene parts of the structure as the height of the tip above the Si substrate or the magnitude of the tip bias was reduced. However, for a Si-terminated tip the calculated current over a methyl-styrene molecule was always higher than that over a styrene molecule (for equal tip heights above the silicon substrate), in contrast to curve L of Fig.6 for an all-tungsten STM tip and to the low bias data in Fig. 2 (a).
- ⁵⁶ The effect of the wave function nodes of the molecular LUMO orbitals on the current profiles in Fig. 8 (where the current corrugation is *reversed* in plots e and h relative to that in l and ll) is clearly more pronounced than that of the molecular HOMO orbitals on the current profiles in Fig. 6 (where the corrugation in plots H is only weakened relative to that in L). We attribute this difference in part to the well known different behavior of the barrier for tunneling between the molecules and an STM tip for positive and negative substrate bias.⁵⁷ When imaging filled sample states, tunneling electrons from the sample with energies just above the tip Fermi-level experience the largest tunnel barrier. The current contribution from higher lying filled

sample states therefore tends to dominate the total tunnel current. In empty state imaging, the situation is reversed. Tunneling electrons originating from the tip Fermi-level experience the lowest tunnel barrier, dominate the tunneling current, and offer a more sensitive probe of empty sample states at that energy. Calculated current profiles are therefore expected to be more sensitive to the details of the sample wave functions at the tip Fermi-energy under positive sample bias. However, in a quantitative analysis of the effect, details of the tip electronic structure must be included as well.

⁵⁷ See J. E. Griffith and G. P. Kochanski, *Ann. Rev. Mat. Sci.* **20**, 219 (1990).

⁵⁸ We note that the overall strength of the calculated transmission is not sensitive to the precise values of the parameters describing the ideal leads (although the *fine* details of the transmission plots depend on these parameters, as in other mesoscopic systems). This is because a rather large number (18) of ideal leads is coupled to each end of the molecular chain whereas the Landauer transmission of the molecular chain is much smaller (less than about 2 in Fig.9, ignoring spin). Thus the molecular chain and its Si substrate (rather than the ideal leads connected to it) constitute the main transport bottleneck in this system, and therefore the precise values of the lead parameters are not very important so long as the choices made for them are reasonable, for example, the band edges for the ideal leads should not be very close to the energy range being studied.

⁵⁹ It should be noted that the quoted height of the carbon atom of the end molecule relative to those of molecules far from the end applies to long molecular chains. Our calculations for short chains yield structures in which the end molecules tilt considerably less towards the silicon substrate.

⁶⁰ The 4th C atom of the benzene ring of the end molecule is located ~ 0.07 Å lower than one of its neighboring C atoms on the same benzene ring but the STM current above that neighboring atom is considerably lower, which we attribute to a destructive quantum interference effect at that site of the benzene ring that has recently been pointed out:⁶² An

electron entering the benzene ring at its 1st carbon atom has two paths that it can take around the ring to its opposite end. Both paths to the 4th C atom have the same length so the interference at that C site is always constructive. But the two paths to the carbon atoms next to the 4th C atom have different lengths so there the interference can be destructive. Thus this mechanism generally favors the 4th C atom.

⁶¹ Currents were evaluated in this case for a vertical tip distance of 3.497 Å above the 4th carbon atom of each benzene ring.

⁶² D. M. Cardamone, C. A. Stafford and S. Mazumdar, (2005) cond-mat/0503540.

⁶³ As noted in Section VIA the conduction mechanism at lower bias is different, mediated by resonant states localized primarily in the Si substrate and adjacent carbon atoms rather than on the molecular HOMO orbitals, thus the tilting of the molecules has a smaller effect on electron transmission between substrate and tip (at constant tip height above the molecule) in the low negative substrate bias regime.

⁶⁴ These band states are discrete because of the finite length of the molecular chain; for an infinite chain they would form a continuum.

⁶⁵ The splitting was also found to be absent when the remainder of the molecular chain is present on the substrate but its direct coupling to the end molecule is switched off by setting the relevant matrix elements of the Hamiltonian and overlap matrix to zero in calculating the transmission.

⁶⁶ The splitting affects the magnitude of the STM current when the tip is over the end of the molecular chain since the tip Fermi level for the value of the applied bias in the inset of Fig. 10 is close to the energy indicated by the arrow, i.e., in the region between the two split peaks of the solid transmission curve.

⁶⁷ Even at low positive substrate bias the apparent height difference between the end and center of the chain is somewhat *smaller* than the geometrical height difference, again contrary to the prediction of the simple variable band gap model.

FIG. 1: (Color on line). Constant current filled-state STM imaging of a methyl-styrene/styrene heterostructure on the H:Si(100) surface. **a**, Growth of the first line segment of methyl-styrene (8L exposure). The chemically reactive silicon radical which initiated the line growth (not shown) is now located at the end of the CH₃-styrene segment (indicated by white arrow). This silicon radical will serve as the initiation site for the growth of the second line segment. **b**, Following a 78 L exposure of styrene, the methyl-styrene segment in panel (a) has been extended to form a molecular heterostructure. The white wedge indicates the location of the heterointerface. At $V_s = -3.0$ V, the methyl-styrene line segment images higher than the styrene segment. **c**, $V_s = -2.4$ V, the methyl-styrene and styrene line segments image with similar height. **d**, $V_s = -1.8$ V, the methyl-styrene and styrene line segments reveal different molecular contrast. Inset: Blue and red arrows show locations of topographic cross-sections presented in Figures 2 (a) and (b), respectively. Images were acquired using a constant tunnel current of 60 pA. Image areas: 8.5 nm×8.5 nm.

FIG. 2: (Color on line). Topographic cross-sections extracted from STM image data of the methyl-styrene/ styrene heterostructure presented in Figure 1. **a**, Topographic cross-sections taken along the chemical attachment points between the heterostructure and the underlying dimer row - along direction of blue arrow in Figure 1 (d). **b**, Topographic cross-sections taken to the right of the trench separating the underlying dimer rows - along direction of red arrow in Figure 1 (d). Cross-sections for a range of sample biases (-3.0 V to -1.8 V) are shown in each panel. Black arrows in panels (a) and (b) indicate the position of the interfacial methyl-styrene molecule.

FIG. 3: (Color on line). Model structure of a heterojunction between methyl-styrene and styrene chains (each of four molecules) on a hydrogen-passivated silicon cluster representing a dimerized H-terminated Si (001) surface. Carbon atoms are black, silicon is blue, hydrogen is white. Inset: Another view of the molecules and nearby substrate atoms.

FIG. 4: (Color on line). Geometry of a methyl-styrene molecule and styrene molecule relaxed using density functional theory on a small dimerized Si (001) cluster. Notation as in Fig.3. For significance of the numbering see text.

FIG. 5: Histogram of the silicon (a), styrene carbon (b), methyl-styrene carbon (c) and hydrogen (d) content of the electronic eigenstates of the eight-molecule styrene/methyl-styrene chain on the hydrogen passivated silicon cluster depicted in Fig.3. The arrows labelled H and L indicate the positions of the tungsten Fermi level relative to the molecular energy spectrum at the negative substrate biases corresponding to current curves H and L, L' in Fig.6. Arrows ll, l, e and h show the tungsten Fermi level at the positive substrate biases corresponding to current curves ll, l, e and h in Fig.8.

FIG. 6: Calculated current I (arbitrary units) flowing between the tungsten STM tip and the styrene/methyl-styrene molecular chain on silicon at some negative substrate biases vs. STM tip position along the chain. The current for curve H has been scaled down by a factor 10. Dotted vertical lines labelled m (s) indicate the locations of the highest carbon atoms of the methyl-styrene (styrene) molecules. The scans are at constant tip height, 2 Å (3 Å) higher than the highest carbon atom of the chain for curves H and L (curve L'). L and L' are at a lower bias, H at a higher bias. The tungsten Fermi level at each bias is indicated by an arrow in Fig.5; see text.

FIG. 7: Calculated current between the tungsten STM tip and the styrene/methyl-styrene molecular chain on silicon vs. STM tip position scanned across the chain, in the direction perpendicular to that of the scans in Fig.6 and 8. Notation as in Fig.6. The scans are at constant tip height of 2 Å higher than the highest carbon atom of the molecular chain. (a) Scan sL (mL) is over the third styrene (methyl-styrene) molecule from the junction for the same bias as scan L in Fig.6. (b) Scan se (me) is over the third styrene (methyl-styrene) molecule from the junction for the same bias as scan e in Fig.8. Each scan passes over the highest carbon atom of the respective styrene or methyl-styrene molecule and crosses the locus of the corresponding scan of Fig.6 or 8 at position = 0.

FIG. 8: Calculated current between the tungsten STM tip and the styrene/methyl-styrene molecular chain on silicon at some positive substrate biases vs. STM tip position along the chain. Notation as in Fig.6 but the scale is the same for all curves. The scans are at constant tip height of 2 Å higher than the highest carbon atom of the molecular chain. The magnitude of the bias voltage increases from curve ll to l to e to h (see text). The tungsten Fermi level at each bias is indicated by an arrow in Fig.5.

FIG. 9: Calculated Landauer transmission probability $T(E)$ (per spin channel) through a molecular chain of 8 styrene molecules on a hydrogen-terminated silicon cluster in the energy range of the molecular LUMO band (a) and of the molecular HOMO band (c). Transmission in the same energy ranges with all Hamiltonian matrix elements and overlaps between orbitals of different molecules switched off (so that transport between the terminal molecules must proceed via the substrate) is shown in plots (b) and (d), respectively.

FIG. 10: Calculated current I (arbitrary units) flowing between the tungsten STM tip and a styrene molecular chain on silicon at some negative substrate biases vs. STM tip position along the chain projected onto an axis parallel to the Si dimer rows of the substrate. The tungsten Fermi level at each bias (L or H) is indicated by an arrow in Fig.5. The styrene molecule at the left end of the chain has been constrained to stand approximately upright in a geometry representative of the region near the center of a molecular chain while the other molecules of the chain have been allowed to relax so that the molecular geometries at right end of the chain are representative of the physical end of a molecular chain on silicon. (See text). The currents for curves H has been scaled up by a factor 5. Dotted vertical lines labelled s indicate the lateral locations of the carbon atoms of the styrene molecules that are furthest from the carbon chains anchoring the molecules to the silicon. The dashed curves are for scans in which the tip passes over each styrene molecule at an equal vertical distance (3.497 Å) above this carbon atom. The solid curves are for scans in which the tip is kept at a constant height above the silicon substrate. Inset: The solid curve shows the Landauer transmission probability between tip and substrate vs. electron energy in eV with the STM tip 3.497 Å above the styrene molecule at the right end of the chain for the same applied bias as curves H. Dashed curve: Same except that all molecules other than the molecule at the right end of the chain are replaced with H atoms passivating the Si substrate. Dot-dashed curve: Landauer transmission probability averaged over tip positions 3.497 Å above the five styrene molecules nearest the left end of the molecular chain.

FIG. 11: Calculated current I flowing between the tungsten STM tip and a styrene molecular chain on silicon at some positive substrate biases vs. STM tip position. The tungsten Fermi level at each bias (l, e and h) is indicated by an arrow in Fig.5. Notation as in Fig. 10.

This figure "figure1.jpg" is available in "jpg" format from:

<http://arxiv.org/ps/cond-mat/0510715v1>

This figure "figure2.gif" is available in "gif" format from:

<http://arxiv.org/ps/cond-mat/0510715v1>

This figure "figure3.jpg" is available in "jpg" format from:

<http://arxiv.org/ps/cond-mat/0510715v1>

This figure "figure4.jpg" is available in "jpg" format from:

<http://arxiv.org/ps/cond-mat/0510715v1>

This figure "figure5.gif" is available in "gif" format from:

<http://arxiv.org/ps/cond-mat/0510715v1>

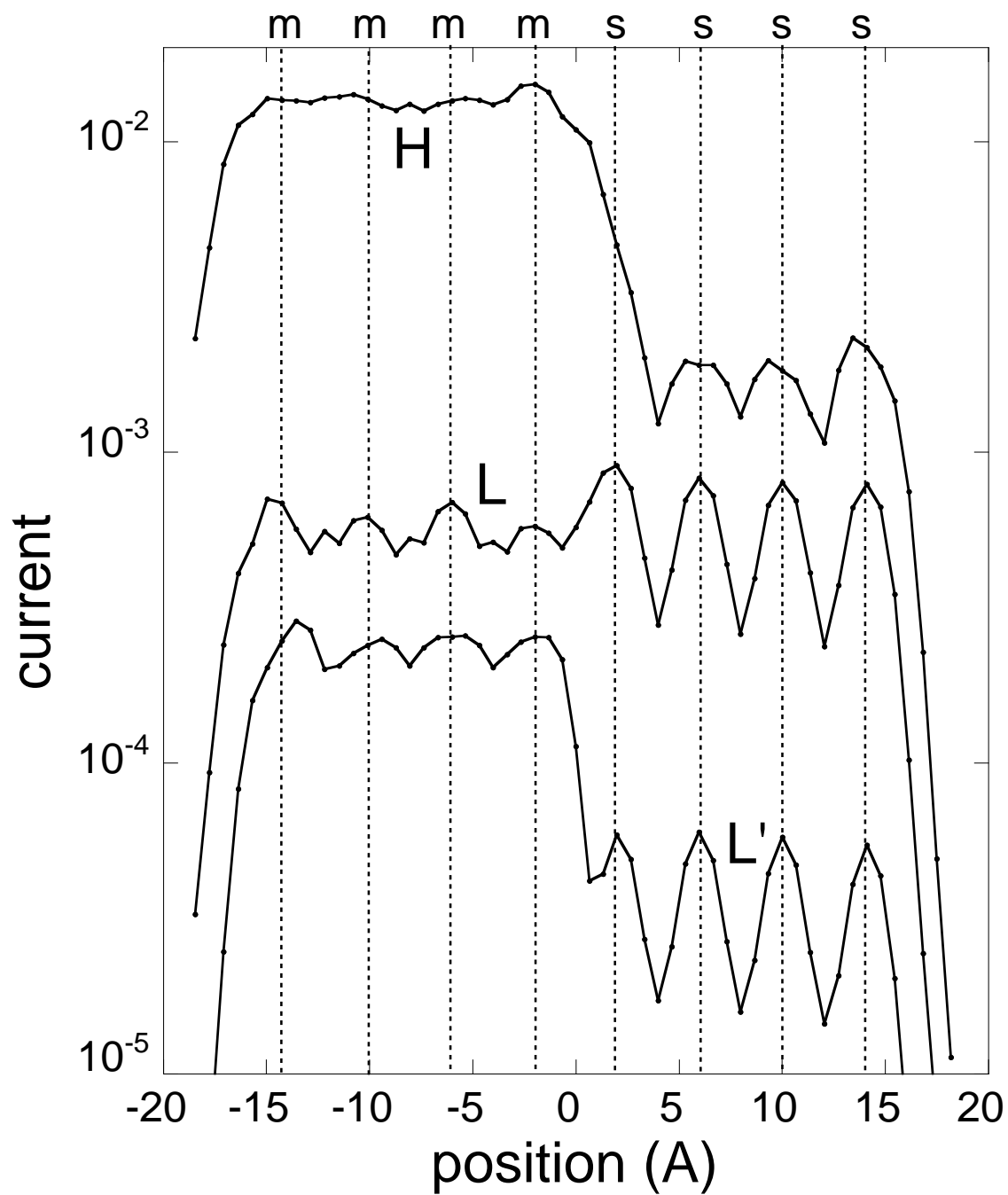


Fig. 6, Kirczenow, Piva, and Wolkow.

This figure "figure7.gif" is available in "gif" format from:

<http://arxiv.org/ps/cond-mat/0510715v1>

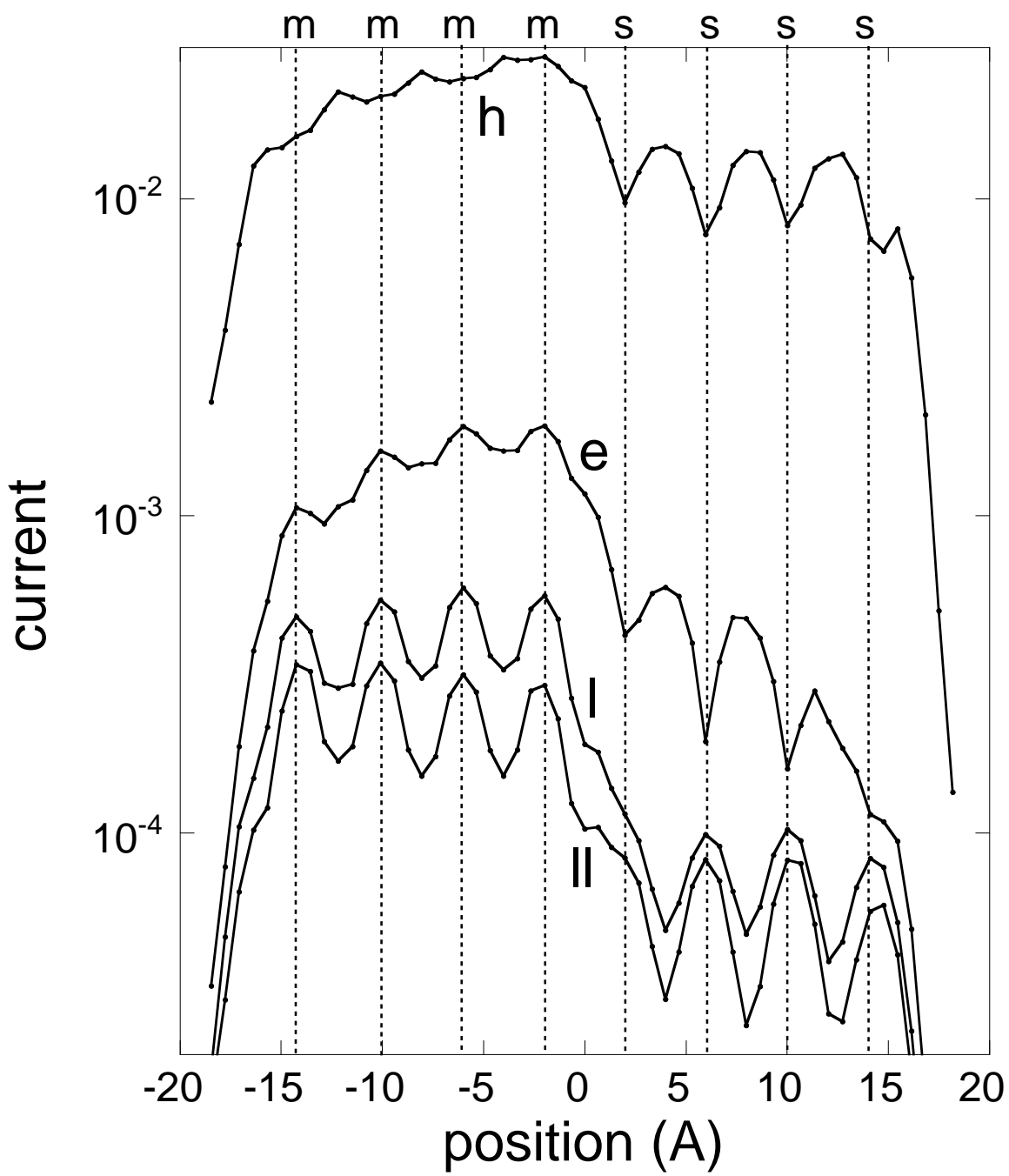


Fig. 8, Kirczenow, Piva, and Wolkow.

This figure "figure9.gif" is available in "gif" format from:

<http://arxiv.org/ps/cond-mat/0510715v1>

This figure "figure10.gif" is available in "gif" format from:

<http://arxiv.org/ps/cond-mat/0510715v1>

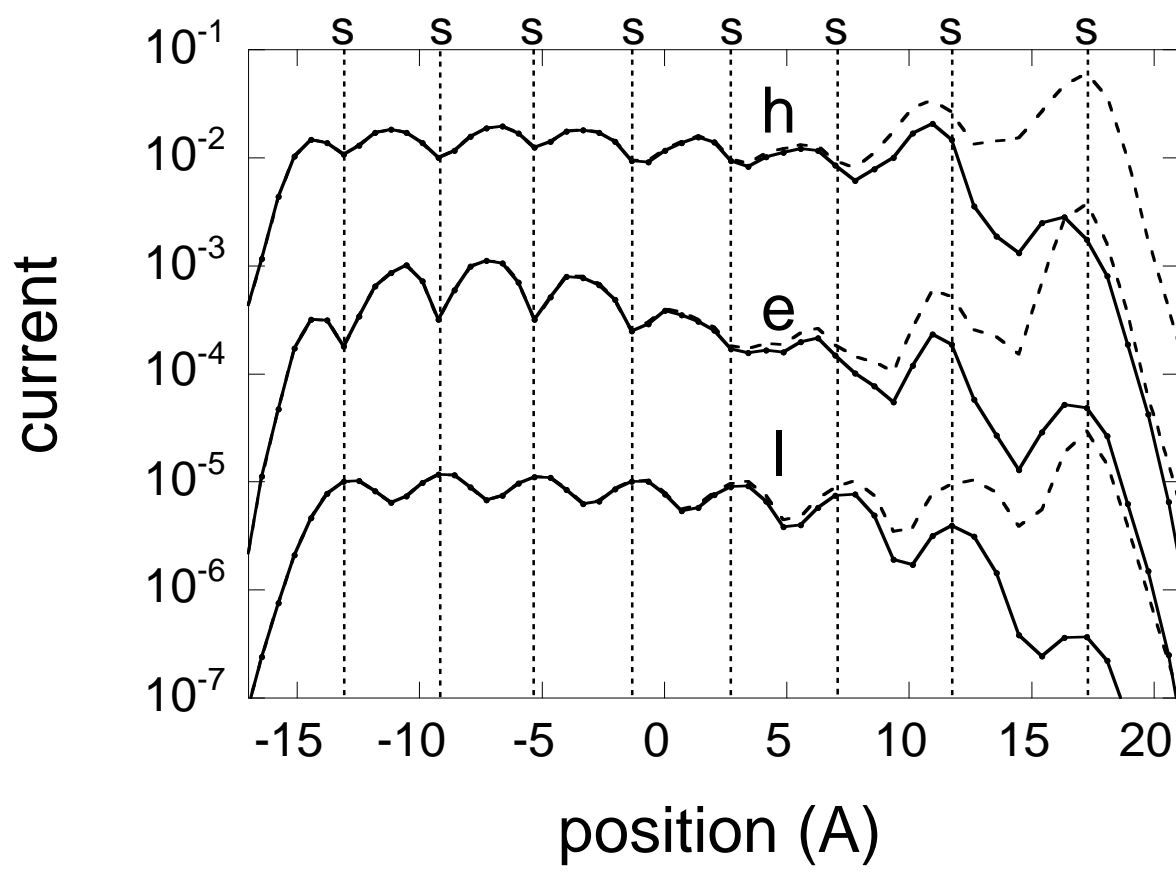


Fig. 11, Kirczenow, Piva, and Wolkow.